Pergamon

Continental Shelf Research, Vol. 17, No. 12, pp. 1483–1511, 1997

0278-4343/97 $17.00 + 0.00

PII: S0278-4343(97)00024-1

Interaction between surface wind and ocean circulation in the Carolina Capes in a coupled low-order model

LIAN XIE,* LEONARD J. PIETRAFESA* and SETHU RAMAN*

(*Received* 28 *May* 1996; *accepted* 31 *January* 1997)

Abstract—Interactions between surface winds and ocean currents over an east-coast continental shelf are studied using a simple mathematical model. The model physics includes cross-shelf advection of sea surface temperature (SST) by Ekman drift, upwelling due to Ekman transport divergence, differential heating of the low-level atmosphere by a cross-shelf SST gradient, and the Coriolis effect. Additionally, the effects of diabatic cooling of surface waters due to air–sea heat exchange and of the vertical density stratification on the thickness of the upper ocean Ekman layer are considered. The model results are qualitatively consistent with observed wind-driven coastal ocean circulation and surface wind signatures induced by SST. This simple model also demonstrates that two-way air–sea interaction plays a significant role in the subtidal frequency variability of coastal ocean circulation and mesoscale variability of surface wind fields over coastal waters. © 1997 Elsevier Science Ltd

1. INTRODUCTION

It has been well documented that freshwater discharge along the coast, the passage of Gulf Stream frontal features and meteorological forcing are the three major causes for the variability of ocean circulation on the continental shelf throughout the southeast U.S. coast, and particularly in the Carolina Capes, from Cape Romain, SC to Cape Hatteras, NC (Pietrafesa *et al.*, 1985; Pietrafesa, 1989; Lee *et al.*, 1989; Atkinson *et al.*, 1989). The continental shelf off the southeast U.S. coast can be divided into three cross-shelf zones, i.e. the inner shelf (0- to 20-m isobath), mid-shelf (21- to 40-m isobath) and the outer shelf (depth > 40 m), according to the physics controlling the subtidal-frequency flow variability (Pietrafesa and Janowitz, 1980; Atkinson *et al.*, 1983). The inner shelf is strongly influenced by weather and coastal boundary forcing, such as freshwater discharge from several rivers. The outer shelf waters are strongly influenced by northward propagating Gulf Stream frontal features and meanders (Pietrafesa *et al.*, 1985; Xie and Pietrafesa, 1995). These events travel to the north along the shelf break at speeds of 40–70 cm s^{-1} with periods of 2–12 days. They appear to result from instabilities within the Gulf Stream that have no well defined, direct relation to local wind forcing (Pietrafesa and Janowitz, 1980; Lee *et al.*, 1989). The most energetic subtidal frequency variance of mid-shelf circulation in the Carolina Capes occurs between 2–10 days which is coincident with the energy peaks of local surface winds (Weisberg and Pietrafesa, 1983; Lee *et al.*, 1985). Thus, the subtidal-frequency variability of mid-shelf circulation in this region is believed to be primarily controlled by

*Department of Marine, Earth and Atmospheric Sciences, Box 8208, North Carolina State University, Raleigh, NC 27695-8208, U.S.A.

local wind forcing during winter (Klinck *et al.*, 1981; Lee *et al.*, 1985; Pietrafesa *et al.*, 1985).

The influence of coastal waters on low-level atmospheric circulation has been investigated in several recent studies (Sweet *et al.*, 1981; Mahrt and Paumier, 1982; Hsu, 1984; Huang and Raman, 1992; Riordan and Lin, 1992). For example, Hsu (1984) showed that the SST gradient across an oceanic frontal feature induces a cross-front pressure gradient which induces a cross-front atmospheric component of flow. Hsu estimated that the velocity induced by this mechanism is roughly 2 m s^{-1} per °C of mean air temperature difference across the SST front. Because of the deflection effect of the Coriolis force, along-shore winds are also generated. This Gulf Stream induced lower-tropospheric circulation is quite similar to the land–sea breeze circulation induced by the land–sea temperature contrast near the coast.

Although the influence of the coastal ocean on the atmosphere and the effect of the latter on the former have long been recognized, the actual coupled interactions between the two fluids are yet poorly understood. Coupled air–sea models have yet to be fully developed for studies of air–sea interactions on the continental shelf. As an attempt toward a better understanding of the coupled air–sea system on the Carolina Capes shelf, a low-order coupled model which includes prognostic equations for SST, ocean current, and surface wind is designed in this study to investigate the interactions between surface winds and shelf ocean circulation.

A low-order model can be formed by truncating the continuous forms of model equations into a series of normal modes or discretizing them in a network of grids, but retaining only the first few modes or a small number of grids. Low-order models have long been used in the study of nonlinear geophysical systems (Lorenz, 1963; Charney and DeVore, 1979). Low-order models have also been used in air–sea interaction studies in the tropics. Vallis (1986) formed a low-order model of El Nino and the Southern Oscillation by simplifying the tropical Pacific as a two-point system. One point is located in the western Pacific and the other is in the eastern Pacific. His two-point model has captured many basic features characteristic of the real system. A great deal of advancement in our understanding of the El Nino/Southern Oscillation phenomenon has been gained by studying the behavior of the coupled tropical atmosphere–ocean system in low-order models (McWilliams and Gent, 1978; Lau, 1981; Cane and Zebiak, 1985; Suarez and Schopf, 1988; Vallis, 1990).

The rationale for using a low-order model to study shelf air–sea interaction off the southeast U.S. coast is that shelf circulation shows considerable coherence within three distinct bands of the shelf, i.e. the inner, middle and outer shelves and distinctly different physical processes control the dynamics of each band (Bumpus, 1973; Weisberg and Pietrafesa, 1983; Lee *et al.*, 1989). Additionally, the relative significance of wind effects to a first-order approximation, is most important over the mid-shelf. Thus, from the air–sea interaction point of view, we may select the mid-shelf as the center of the field of grids while treat the conditions in the inner and outer shelves as non-local boundary force controlled by land–sea boundary processes on the coastal side and by the Gulf Stream on the offshore side, respectively. Details of model formulation will be presented in Section 2. Section 3 will be devoted to the analysis of model results. In Section 4, results from approximated forms of the model will be examined. A brief discussion is contained in Section 5 followed by a concluding section.

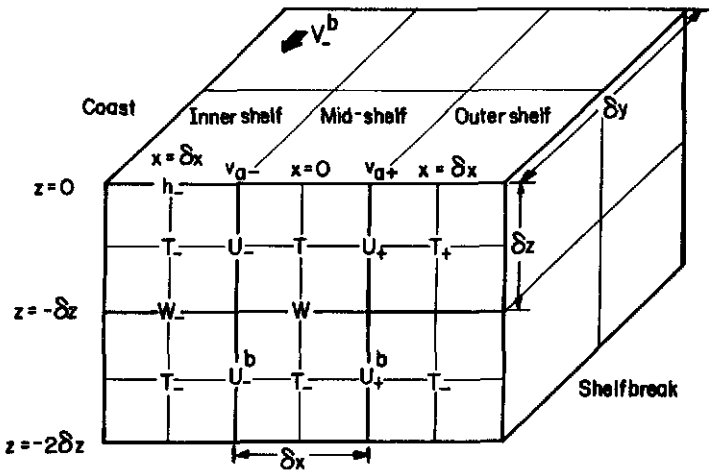

Fig. 1. A schematic diagram of the spatial structure of the low-order model.

2. MODEL EQUATIONS

2.1. *The ocean*

We will consider a simplified sea–air system over the continental shelf which is assumed bounded to the west by a straight north–south coast (Fig. 1). For convenience, before we present the model, we list in the following, some symbols which will be used in the model equations. They are:

T_-, T, T_+: SST over the inner, middle and outer shelves, respectively;
U_-, U, U_+: cross-shelf surface ocean currents over the inner, middle and outer shelves, respectively;
V_-, V, V_+: along-shelf surface ocean currents over the inner, middle and outer shelves, respectively;
W_-, W, W_+: vertical velocities at the mid-depth over the inner, middle and outer shelves, respectively;
U_-^b, U^b, U_+^b: near-bottom ocean currents over the inner, middle and outer shelves, respectively;
h_-: free-surface elevation over the inner shelf; and
V_-^N: along-shelf current over the inner shelf at a point north of the model section.

The surface ocean currents over the middle shelf are diagnostic quantities which are interpolated linearly from corresponding velocities over the inner and outer shelves, i.e. $U = 0.5(U_- + U_+)$, $U^b = 0.5(U_-^b + U_+^b)$. The governing equations of the ocean model are presented below.

Consider first, the continuity equation

$$\frac{\partial u}{\partial x} + \frac{\partial v}{\partial y} + \frac{\partial w}{\partial z} = 0.$$

Over the mid-shelf, we assume the vertical velocity at the sea-surface is zero (rigid lid) and the along-shelf current is uniform. Then, the continuity equation can be written in finite

difference form as

$$\frac{U_+ - U_-}{\delta x} - \frac{W}{\delta z} = 0. \tag{1}$$

Equation (1) states that if the cross-shelf surface current over the outer shelf is onshore and greater than that over the inner shelf, downwelling would occur over the mid-shelf and vice versa.

Over the inner shelf, sea level change may not be neglected because of the effect of the coast. Assuming the current normal to the coast is zero at the coast ($x = -1.5\delta x$), the continuity equation for the inner shelf becomes

$$\frac{dh_-}{dt} = W_- - \frac{\delta z}{\delta x} U_- - \frac{\delta z}{\delta y}(V_-^N - V_-). \tag{2}$$

The vertical velocity at the mid-depth of the inner shelf water (W_-) can be estimated by the bottom layer convergence there as:

$$W_- = -\frac{\delta z}{\delta x} U_-^b. \tag{3}$$

Replacing W_- in equation (2) by equation (3), we have

$$\frac{dh_-}{dt} = -\frac{\delta z}{\delta x}(U_- + U_-^b) - \frac{\delta z}{\delta y}(V_-^N - V_-). \tag{4}$$

The first term in equation (4) represents the effect of barotropic cross-shelf divergence on the variation in coastal sea-level. If the mean (barotropic) cross-shelf flow is onshore (offshore), coastal sea level rises (sinks). The second term represents the effect of along-shelf divergence on coastal sea-level variations. Under the condition of southward along-shelf currents, if the upstream current velocity is weaker than that in the study region, along-shelf divergence would occur near the coast which depresses the sea level at the coast, and vice versa. Equation (4) also indicates that if h reaches steady state, along-shelf divergence would induce onshore flow to maintain the mass balance over the inner shelf. In more realistic situations, with the inclusions of bottom slope and current vorticity, motions induced by bottom topography and Ekman pumping should be included in equation (4). For simplicity, these effects are not included in the present model.

Assume the temperature at the mid-shelf is determined by cross-shelf advection, upwelling and air–sea heat exchange. Navafacial heat exchange can be simply parameterized by a Newtonian cooling effect with a time scale σ^{-1}. Let T* be the temperature to which the mid-shelf SST would relax in the absence of motion. Then the thermodynamic equation written in continuous form is

$$\frac{\partial T}{\partial t} = -u\frac{\partial T}{\partial x} - w\frac{\partial T}{\partial z} - \sigma(T - T^*)$$

which can be discretized, using a centered difference scheme, as

$$\begin{aligned} \frac{dT}{dt} &= -U\frac{(T_+ - T_-)}{2\delta x} - W\frac{(T - T_-)}{\delta z} - \sigma(T - T^*) \\ &= -(U_+ + U_-)\frac{(T_+ - T_-)}{4\delta x} - (U_+ - U_-)\frac{(T - T_-)}{\delta x} - \sigma(T - T^*). \end{aligned} \tag{5}$$

Equation (5) describes the mid-shelf SST change caused by cross-shelf advection and surface cooling and is linear if the cross-shelf ocean currents are induced by a constant wind stress. This would be the case for an uncoupled ocean forced by a uniform large-scale wind, sufficiently far away from the coast. If the ocean is coupled to the atmosphere, the change of SST would induce a change in the surface wind field and consequently a change in the cross-shelf current field. In this case, equation (5) becomes nonlinear.

The simplest assumption to make about the surface ocean current is that it is mechanically forced by surface wind stress. In this case, the equations governing the classical Ekman solution can be applied. Denote u, v as the x and y components of the surface current. Then the x, y horizontal momentum equations written in continuous form are

$$(x)\quad \frac{\partial u}{\partial t} = -g\frac{\partial h}{\partial x} + fv + \frac{\partial \tau_x}{\partial z} - \nu u$$

$$(y)\quad \frac{\partial v}{\partial t} = -g\frac{\partial h}{\partial y} - fu + \frac{\partial \tau_y}{\partial z} - \nu v$$

where (τ_x, τ_y) are the shear stresses within the surface Ekman layer, and ν^{-1} is a frictional time scale for the shelf waters. In the real coastal ocean, the shallow inner shelf tends to be well mixed during winter and significant damping due to bottom friction exists there. In the middle and outer shelves, friction is induced at both the surface and bottom, via surface and bottom stresses and vertical mixing. The value of ν for the inner shelf may be larger than that for the mid and outer portions of the shelf (Janowitz and Pietrafesa, 1980). However, for simplicity, we will assume a constant ν for the entire shelf and discuss the sensitivity of model results to the choice of ν later in the text. We next denote H and H_+ as the Ekman layer thicknesses over the middle and the outer shelves, respectively and assume that they decrease as the vertical temperature contrast (stratification) increases, i.e.

$$H = D/[1 + k(T - T_-)] \tag{6}$$

$$H_+ = D/[1 + k(T_+ - T_-)] \tag{7}$$

where k is a constant representing the effect of vertical stratification on the Ekman depth, and D is the unperturbed Ekman depth. For simplicity, the Ekman layer depth over the inner shelf (H_-) is assumed to be the same as that over the middle shelf. In the special case of $k = 0$, $H_+ = H = H_-$, which represents a constant Ekman depth across the entire shelf. Next, integrating the momentum equations vertically through the Ekman layer, writing them in finite difference form, and assume the following linear wind stress relationship between the drag coefficient (r) and surface winds over the inner (u_{a-}, v_{a-}) and outer shelf (u_{a+}, v_{a+})

$$\tau_+^x = ru_{a+} \tag{8}$$

$$\tau_-^x = ru_{a-} \tag{9}$$

$$\tau_+^y = rv_{a+} \tag{10}$$

$$\tau_-^y = rv_{a-} \tag{11}$$

we have

$$\frac{dU_+}{dt} = fV_+ + \frac{ru_{a+}}{D}[1 + k(T_+ - T_-)] - vU_+ \tag{12}$$

$$\frac{dU_-}{dt} = g\frac{h_-}{\delta x} + fV_- + \frac{ru_{a-}}{D}[1 + k(T - T_-)] - vU_- \tag{13}$$

$$\frac{dV_+}{dt} = -fU_+ + \frac{rv_{a+}}{D}[1 + k(T_+ - T_-)] - vV_+ \tag{14}$$

$$\frac{dV_-}{dt} = -fU_- + \frac{rv_{a-}}{D}[1 + k(T - T_-)] - vV_-. \tag{15}$$

We assume the total water column is sufficiently deep so that the wind stress does not act directly on the bottom water. In this case, the momentum equations for U_-^b and V_-^b are

$$\frac{dU_-^b}{dt} = g\frac{h_-}{\delta x} + fV_-^b - vU_-^b \tag{16}$$

$$\frac{dV_-^b}{dt} = -fU_-^b - vV_-^b \tag{17}$$

Assuming no net convergence for the entire water column over the middle shelf, we have

$$U_+^b = -U_+ + U_- + U_-^b \tag{18}$$

which can be used to diagnose the bottom current over the outer shelf.

2.2. *The atmosphere*

Consider a two-dimensional atmosphere uniform in y. Denote u'_{a-}, u'_a, *and* u'_{a+} as the cross-shelf perturbation wind components over the inner, middle and outer shelves, respectively, and the corresponding along-shelf wind components as v'_{a-}, v'_a, v'_{a+}. Then the linearized momentum equations for the surface winds are

$$\frac{du'_{a+}}{dt} = fv'_{a+} + \Pi(T_+ - T) - \mu u'_{a+} \tag{19}$$

$$\frac{du'_{a-}}{dt} = fv'_{a-} + \Pi(T - T_-) - \mu u'_{a-} \tag{20}$$

$$\frac{dv'_{a+}}{dt} = -fu'_{a+} - \mu v'_{a+} \tag{21}$$

$$\frac{dv'_{a-}}{dt} = -fu'_{a-} - \mu v'_{a-} \tag{22}$$

where Π is a constant representing the effect of cross-shelf SST gradient on the surface pressure gradient force and μ is a Rayleigh friction coefficient for the surface wind. Based on

the estimate of Hsu (1988) for mesoscale circulations over the Gulf Stream at a latitude of roughly 37°N, the typical values for Π and μ are $\Pi = 6.4 \times 10^{-5}$ m s^{-2} deg^{-1}, and $\mu = 3.2 \times 10^{-5}$ s^{-1}.

2.3. *Air–sea coupling*

The atmosphere and the ocean over the shelf are coupled through surface wind stress acting on the sea surface and a thermodynamic forcing on the atmosphere caused by the diabathic SST gradient. Assuming the ambient cross-shelf wind is u_{am} and the along-shore wind is v_{am}, then the total cross-shelf and along-shore wind components over the inner and outer shelves (u_{a-}, v_{a-} and u_{a+}, v_{a+}) are the sum of (u_{am}, v_{am}) and the perturbation winds (u'_{a-}, v'_{a-} and u'_{a+}, v'_{a+}).

The coupled system consists of 12 prognostic equations [equations (4), (5), (12), (13), (14), (15), (16), (17), (19), (20), (21) and (22) and two diagnostic equations [equations (3) and (18)]. The system is closed if T_+, T_- and V_-^N are assumed to be known boundary values. In this case, T_- and T_+ can be considered as the western and eastern boundary conditions which may be assumed to be time-dependent parameters. For example, a time-dependent T_+ may represent a temporally varying temperature field associated with the Gulf Stream flowing along the eastern edge of the shelf. A more involved (but straight forward) development is to introduce two additional prognostic equations similar to equation (5) for T_+ and T_-, respectively. Then, we will need to specify cross-shelf currents at the coast (which can certainly be assumed as zero), and at the shelf edge which may be assumed as the cross-shelf current induced by Gulf Stream meanders. In this study, we will simply assume T_+ and T_- as known constants. Parameter V_-^N represents the convergence effect associated with along-shelf current variability. This effect can be caused either by an irregular coastal shape or by a wind stress which is variable in the along-shelf direction. This term is included in the model to allow a parameterization of the effect of along-shelf divergence on the cross-shelf transport.

If $k = 0$, the uncoupled atmosphere and ocean are both linear. In this case, the only nonlinear equation in the coupled system is equation (5). When $k \neq 0$, additional nonlinearity enters the coupled system through equations (6) and (7). Because of the nonlinearity, the coupled system cannot be solved analytically, in general. In the following section, we present the numerical solutions to the coupled system.

3. RESULTS

3.1. *Shelf circulation and surface winds in the coupled system*

The numerical algorithm of Gear (1971) is used to solve the model equations. In all experiments, unless otherwise specified, the following characteristic parameters are used: $\delta x = 4 \times 10^4$ m, $\delta z = 20$ m, $\delta y = 2.5 \times 10^5$ m, $V_-^N = u_{am} = 0$ m s^{-1}, $f = 8.15 \times 10^{-5}$ s^{-1}, $r = \mu = 2.59 \times 10^{-5}$ s^{-1}, $\nu = 5.19 \times 10^{-6}$ s^{-1}, $\sigma = 2.59 \times 10^{-6}$ s^{-1}, $\Pi = 5.2 \times 10^{-5}$ m s^{-2}deg^{-1}, $v_{am} = -3.5$ m s^{-1}, $T_- = 8.5$°C, $T_+ = 20$°C, $T^* = T_i = 8.5$°C, $k = 2.2 \times 10^{-2}$ deg^{-1}.

The values of drag (r) and friction coefficient (μ) at the air–sea interface are assumed identical which are of the time scale of roughly half a day. The value of ν corresponds to an oceanic damping time scale of approximately 2 days. The thermal relaxation time scale

(σ^{-1}) is about 5 days. The time scale for the surface wind to respond to the SST forcing (Π^{-1}) is on the order of 5 h, a value equivalent to that suggested by Hsu (1984). The value of k assumes a 2 m reduction of the surface Ekman-layer depth if the water temperature at the sea surface (upper layer) is 5°C warmer than the interior (bottom layer). These model parameters are selected to be characteristic of the SAB marine atmosphere and ocean margin oceanography from the extensive existing literature, though each can vary. Sensitivity of the model to these parameters are examined in the following and in Section 5 to provide assurance that the results generated by the model will remain qualitatively correct, even as the model parameters change within a reasonable range.

3.1.1. *Cross-shelf surface winds.* The ambient wind has no cross-shelf component ($u_{am}=0$), so total cross-shelf winds are the perturbation winds produced by oceanic thermal forcing. Figure 2a shows the cross-shelf winds over the inner- and outer-shelves (u'_{a-} and u'_{a+}) during a 10-day period. Both increase offshore from a zero velocity. During the first 5 h, u_{a+} accelerates offshore rapidly from zero to approximately 6 m s^{-1}, in apparent response to the large initial SST difference between the outer shelf and the mid-shelf. During this period, surface winds over the inner shelf do not vary much because, initially there is no cross-shelf SST contrast between the inner- and mid-shelves. During the next 10 h, u'_{a+} decreases from 6 m s^{-1} to about 0.3 m s^{-1}. This is caused primarily by an inertial oscillation as will be explained later when we discuss the along-shore winds. The surface wind speed over the inner shelf increases continuously during the first inertial period (approximately 22 h). By the end of the third inertial period, the maximum cross-shelf wind over the inner shelf reaches a quasi-steady value of approximately 1 m s^{-1} flowing offshore. The cross-shelf surface wind over the outer shelf also oscillates at the local inertial period with decreasing amplitude. By the end of the third inertial period, its amplitude reaches a quasi-steady state value of roughly 1.7 m s^{-1} blowing offshore. Apart from the effect of friction, the deceleration of u'_{a+} after the first a few hours is caused by the warming of mid-shelf water induced by onshore warm water penetration, to be discussed later. The same process is also responsible for the offshore acceleration of the surface wind over the inner shelf.

3.1.2. *Along-shelf surface winds.* The along-shelf surface perturbation winds (v'_{a-} and v'_{a+}) over the inner and outer shelves during the 10-day period are shown in Fig. 2b. Again, an inertial oscillation is apparent. Apart from the inertial oscillation, there exist opposite trends for the along-shelf winds over the inner- and outer-shelves. The along-shelf wind over the outer shelf accelerates southward rapidly from zero to approximately 9 m s^{-1} during the first 5 h which clearly indicates the atmosphere tends to adjust itself geostrophically to the large cross-shelf pressure gradient associated with the initial cross-shelf SST gradient between the mid- and outer-shelves. This southward along-shelf wind component requires a strong onshore Coriolis force to balance the cross-shelf pressure gradient and thus, causes a rapid reduction of offshore wind speed over the outer shelf after the first 5 h, as shown in Fig. 2a. After the first 5 h, v'_{a+} oscillates at the local inertial period and decreases in magnitude in response to both friction and a reduction of the cross-shelf SST gradient between the mid- and outer-shelves. At the end of the third inertial period, v'_{a+} decreases to a value of about -5 m s^{-1}. The value of v'_{a-} undergoes a trend opposite to that of v'_{a+}. It also oscillates at the local inertial period but displays a tendency to accelerate southward. At the end of the third inertial period, it reaches a value of about -2.5 m s^{-1}.

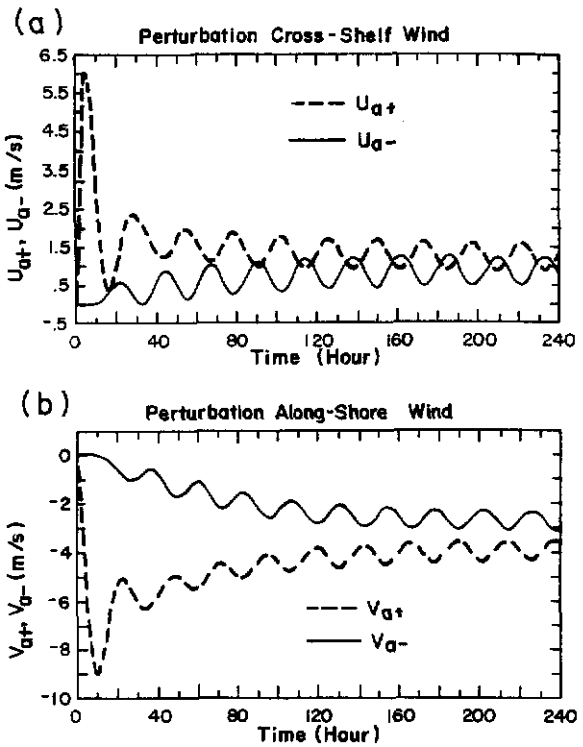

Fig. 2. Evolution of surface perturbation winds over the inner shelf (solid curve) and outer shelf (broken curve) in a coupled low-order model with varying depth for the upper-ocean Ekman layer ($k = 0.022$ deg^{-1}, see text for detail); (a) cross-shelf perturbation winds; (b) along-shelf perturbation winds.

3.1.3. *Cross-shelf surface currents and mid-shelf vertical velocity.* Cross-shelf surface currents (U_- and U_+) over the inner- and outer- shelves are calculated starting from a quiescent initial state. Figure 3a shows the evolution of U_- and U_+ during the 10-day period. The surface current over the outer shelf accelerates offshore during the first few hours in response to the initial offshore wind there. The surface current then turns and drifts onshore rapidly. After approximately 17 h, a maximum onshore current of 0.46 m s^{-1} is reached over the outer shelf. The corresponding cross-shelf current over the inner shelf reaches roughly 0.1 m s^{-1} onshore after approximately 12 h. Both currents then oscillate at the local inertial period. The outer shelf current undergoes a decreasing trend in amplitude while the inner shelf current undergoes an increasing trend. The mean onshore current speed is larger over the outer shelf than the mean onshore current over the inner shelf; though the two gradually approach each other. This current speed difference produces a surface convergence over the mid-shelf which could facilitate mid-shelf frontogenesis. Meanwhile, a downwelling trend is induced over the mid-shelf by the surface convergence there (Fig. 3b). The vertical velocity also undergoes an inertial oscillation and shows a net downwelling. Its mean value gradually decreases to zero as the cross-shelf surface currents over the inner- and outer-shelves approach each other.

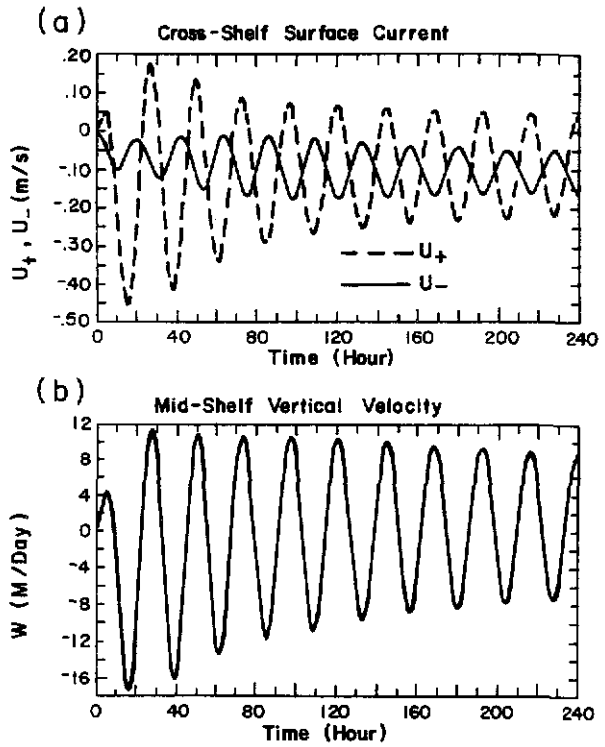

Fig. 3. Same as Fig. 2 but for the cross-shelf surface currents and mid-shelf vertical velocity; (a) cross-shelf surface currents over the inner shelf (solid curve) and outer shelf (broken curve); (b) mid-shelf vertical velocity at the mid-depth ($z = -\delta z$).

3.1.4. *Cross-shelf bottom currents and coastal upwelling.* The cross-shelf, bottom currents over the inner- and outer-shelves (U_-^b and U_+^b) are shown in Fig. 4a. Both U_-^b and U_+^b show strong inertial oscillations and a mean offshore velocity. The cross-shelf bottom current is stronger over the outer shelf than over the inner shelf which creates a divergence at the bottom over the mid-shelf, facilitating downwelling there. Such a divergence decreases with time. During the first couple of days, the mean inner shelf bottom current is less than 0.05 m s^{-1} while the mean outer shelf bottom current is generally greater than 0.15 m s^{-1}. But by the end of the third inertial period, the mean speed of the cross-shelf bottom current approaches approximately 0.1 m s^{-1} over both the inner and outer shelves. However, the amplitude of the outer shelf current remains greater than that over the inner shelf.

The net onshore surface current and offshore bottom current over the inner shelf produce a net downwelling near the coast (Fig. 4b). Although oscillating at the local inertial period, the mean downwelling rate increases with time and eventually reaches a quasi-steady state. By the end of the third inertial period, the mean coastal downwelling rate is approximately 4 m day^{-1}.

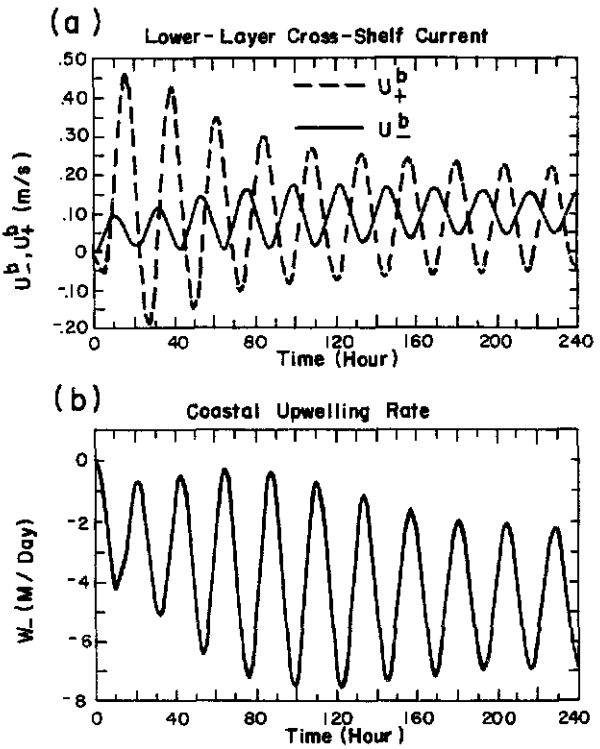

Fig. 4. Same as Fig. 3 but for lower-layer cross-shelf currents and coastal (inner shelf) upwelling; (a) cross-shelf surface currents over the inner shelf (solid curve) and outer shelf (broken curve); (b) inner-shelf vertical velocity at the mid-depth ($z = -\delta z$).

3.1.5. *Coastal sea level and along-shore currents.* The onshore surface current over the inner shelf does not exactly balance the offshore bottom current there, particularly during the first couple of days. The two current regimes are controlled by different physical processes. The surface current is controlled primarily by the along-shelf wind stress component and the diabathic or cross-shelf pressure gradient associated with coastal sea level change, while the bottom current is primarily determined by bottom friction and the barotropic pressure gradient associated with the diabathic slope of coastal sea level. Additionally, the Coriolis force induces inertial oscillations which are gradually damped by friction. During the first 2 days, the mean inner shelf cross-shelf surface current is greater than 0.05 m s^{-1} while the counterpart near the bottom is generally less than 0.05 m s^{-1}. This creates a barotropic convergence near the coast which then causes a sea level rise (Fig. 5a). As the barotropic convergence near the coast decreases, sea level at the coast gradually reaches a quasi-steady state height of 27 cm.

Since the rigid lid approximation is used over the mid- and outer-shelves, sea level only changes over the inner shelf. This is not an unreasonable assumption because wind-induced sea level change primarily occurs within one Rossby deformation radius from the coast, which in our case would be within the width of the inner shelf. The rise of sea level at the

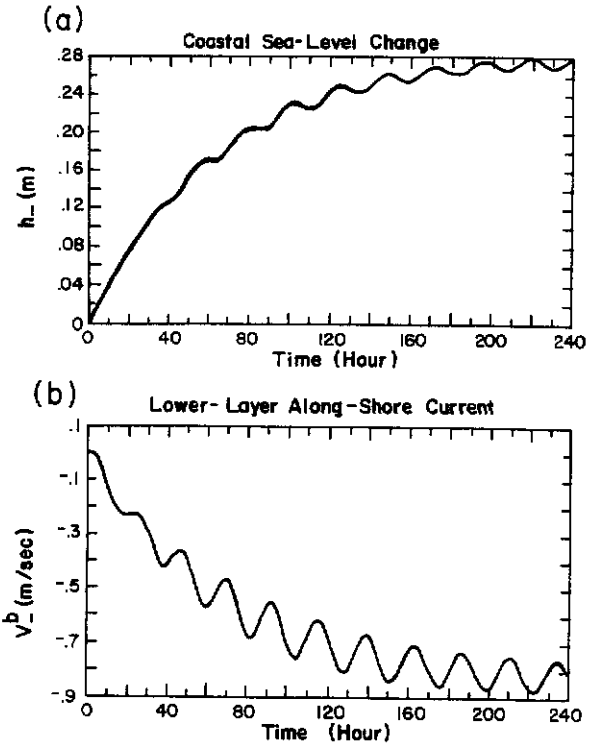

Fig. 5. Same as Fig. 3 but for coastal sea-level change (panel a) and lower-layer along-shelf current (panel b).

coast produces a barotropic pressure gradient which consequently sets up a southward barotropic along-shelf geostrophic current over the inner shelf (Fig. 5b). This current strengthens with time until the diabathic pressure gradient caused by coastal sea level reaches a steady state. By then, the coastal geostrophic current reaches a steady state value of approximately 0.8 m s^{-1}. At the end of the third inertial period, the coastal along-shelf current is roughly 0.55 m s^{-1}, southward.

3.1.6. *Mid-shelf SST.* Of central importance to air–sea coupling over the shelf is the evolution of the SST over the mid-shelf (Fig. 6). It is shown that the mid-shelf perturbation SST increases rapidly initially and then gradually reaches a quasi-steady state value of roughly 4.5°C. The warming of mid-shelf SST can be expected from the onshore surface cross-shelf current and the basic SST gradient which increases seaward. In addition to the warming trend, an inertial oscillation with an amplitude of about 0.5°C appears in the mid-shelf SST field.

3.2. *The case of* k = 0

The effect of surface Ekman layer depth variation induced by vertical temperature stratification can be examined by setting $k = 0$ and comparing the results to those obtained

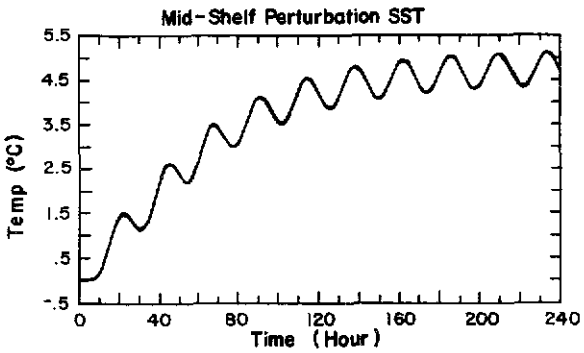

Fig. 6. Mid-shelf perturbation SST in the coupled model.

for $k = 0.022\ \text{deg}^{-1}$ discussed in the previous section. The transient solutions for the perturbation along-shelf wind, cross-shelf surface current, mid-shelf upwelling rate and mid-shelf perturbation SST for $k = 0$ are plotted respectively in Fig. 7a,b,c and d. There is little difference between the along-shelf surface winds for $k = 0$ (Fig. 7a) and $k = 0.022\ \text{deg}^{-1}$ (Fig. 2b) during the first few days. However, the amplitudes of the inertial oscillation and the steady state wind speeds show marked differences between the two cases. The amplitude of the inertial oscillation is larger for $k = 0.022\ \text{deg}^{-1}$ than for $k = 0$. The quasi-steady state (day ten) along-shelf wind speed over the inner-shelf for $k = 0$ is about $2.3\ \text{m s}^{-1}$ (Fig. 7a) which is slightly less than the corresponding wind speed for $k = 0.022\ \text{deg}^{-1}$ ($3\ \text{m s}^{-1}$, Fig. 2b). The quasi-steady state (day ten), along-shelf wind speed over the outer shelf is larger for $k = 0$ ($4.3\ \text{m s}^{-1}$, Fig. 7a) than for $k = 0.022\ \text{deg}^{-1}$ ($3.5\ \text{m s}^{-1}$, Fig. 2b). The difference between the cross-shelf current for $k = 0$ (Fig. 7b) and that for $k = 0.022\ \text{deg}^{-1}$ (Fig. 3a) appears primarily over the outer shelf. There, the cross-shelf current is larger for $k = 0.022\ \text{deg}^{-1}$ than for $k = 0$. The same is true for the inertial oscillation amplitude (with a difference of approximately $10\ \text{cm s}^{-1}$). The effect of stronger onshore current over the outer shelf for $k = 0.022\ \text{deg}^{-1}$ must enhance the mid-shelf downwelling rate. This can be verified by comparing Fig. 3b to Fig. 7c. The maximum downwelling for $k = 0.022\ \text{deg}^{-1}$ at the peak of the first inertial period reaches $17\ \text{m day}^{-1}$ while the corresponding value for $k = 0$ is $13\ \text{m day}^{-1}$. The former also showed a larger inertial amplitude than the latter. The effect of the stronger onshore current over the outer shelf for $k = 0.022\ \text{deg}^{-1}$ also appears in the mid-shelf SST field (Fig. 7d). Because of the stronger onshore current over the outer shelf and thus, stronger warm water advection toward the mid-shelf, the mid-shelf SST is roughly 1°C warmer for $k = 0.022\ \text{deg}^{-1}$ than for $k = 0$ at the end of the 10-day period. During the first 2 days, however, the difference is roughly half of that value (0.5°C). The cooler mid-shelf water for $k = 0$ explains why the along-shelf winds are stronger over the outer shelf for $k = 0$ than for $k = 0.022\ \text{deg}^{-1}$ while the opposite is true for the along-shelf wind over the inner shelf.

It is clear that vertical temperature stratification has an effect on the solution of the coupled system. However, compared to the total perturbation wind, ocean current and mid-shelf perturbation SST, the modulations of respective variables by the stratification effect are secondary and do not change the solution qualitatively. Thus, in the following, we will set $k = 0$ and focus on the effect of air–sea coupling.

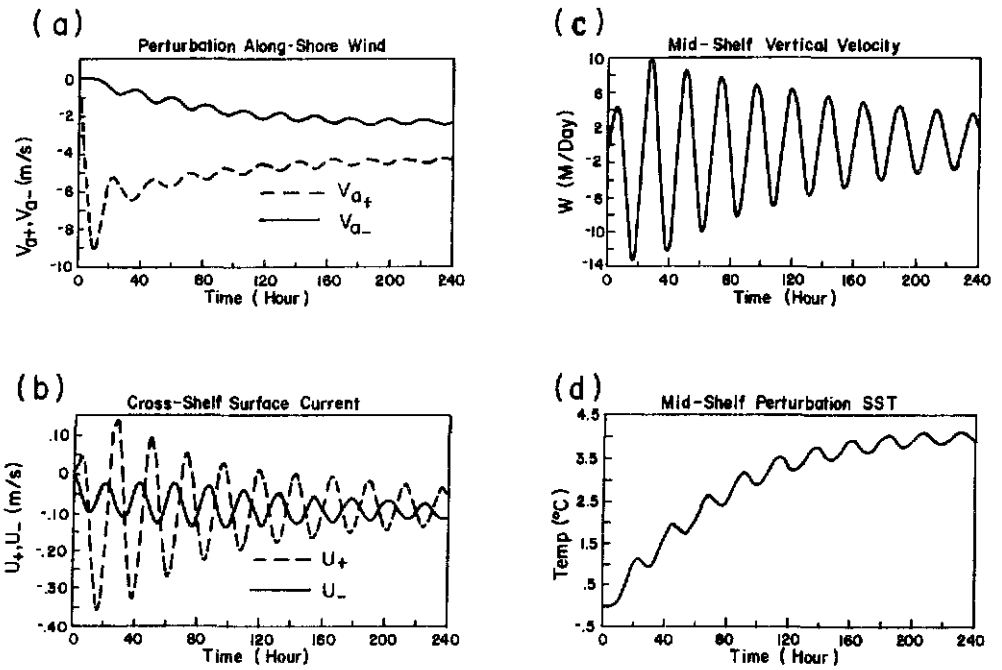

Fig. 7. Evolution of surface winds and ocean circulation in a coupled low-order model with constant Ekman layer depth ($k=0$); (a) perturbation along-shelf surface wind speed over the inner shelf (solid curve) and the outer shelf (broken curve); (b) cross-shelf surface current speed over the inner shelf (solid curve) and the outer shelf (broken curve); (c) mid-shelf vertical velocity at the mid-depth; (d) mid-shelf perturbation SST.

3.3. *The uncoupled case*

The effect of air–sea coupling on the ocean current and surface winds over the continental shelf can be examined by contrasting the results for $\Pi = 5.29 \times 10^{-5}$ m s^{-2} deg^{-1} with those for $\Pi = 0$. Setting $\Pi = 0$ effectively decouples the atmosphere from the ocean. From an oceanographic point of view, this is equivalent to the use of a large-scale ambient wind to calculate the wind stress and set it as a time-independent constant. Figure 8a–d shows coastal sea-level change, cross-shelf ocean currents, mid-shelf vertical velocity, and mid-shelf SST, respectively. Clearly, in all fields, the mean value and amplitude of the oceanic variables are considerably less than their counterparts in the coupled case. The mid-shelf perturbation SST, for example, reaches only 1.7°C which is roughly one-third of the value in the coupled case. Thus air–sea coupling is important for the variability of shelf ocean circulation and SST. From the atmospheric point of view, the feedback from the ocean is the cause for along-shelf wind acceleration (deceleration) under northerly (southerly) ambient wind conditions. This is perhaps a cause for the low-level jets frequently observed along oceanic SST fronts (Doyle and Warner, 1990, 1993).

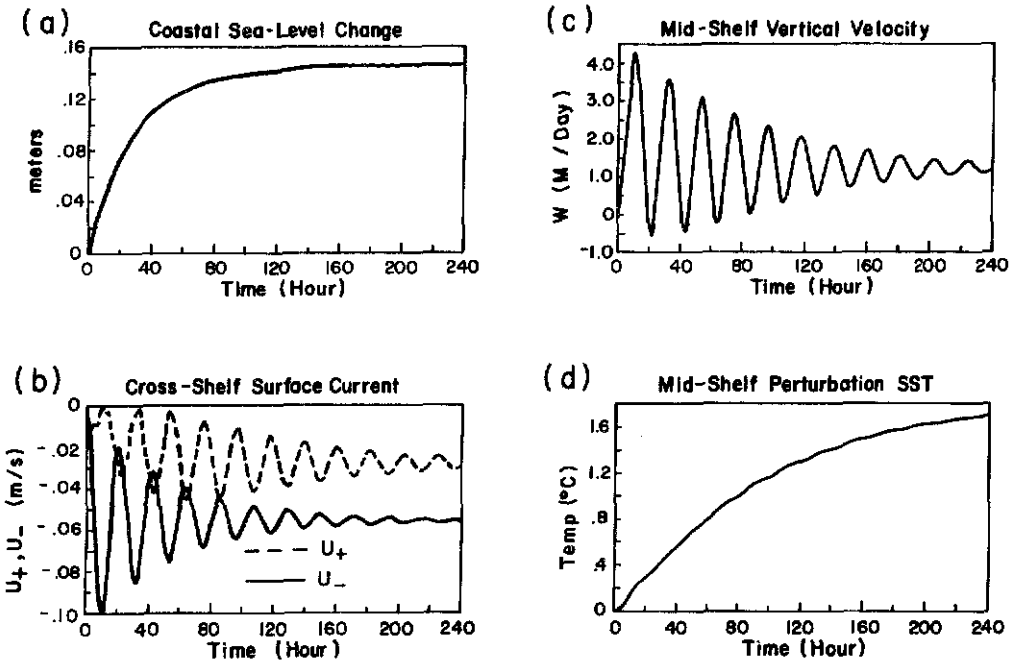

Fig. 8. Same as Fig. 7 but for the uncoupled case ($a=0$) in which surface wind does not change with time; (a) coastal sea-level change; (b) cross-shelf surface currents over the inner shelf (solid curve) and the outer shelf (broken curve); (c) mid-shelf vertical velocity at the mid-depth; (d) mid-shelf perturbation SST.

4. APPROXIMATE SOLUTIONS

In this section, we will discuss the applicability of several approximations to the coupled system. In the following discussion, we will set $k=0$, $V_-^N = V_-$, and invoke a rigid lid over the entire shelf.

4.1. *Rigid lid approximation*

Assume the barotropic divergence is zero over the entire shelf (rigid lid approximation). Then the effect of coastal sea level is excluded. In this case, the coupled system (See Appendix A) is closed without the equations for coastal sea level (equation (4)), and the inner shelf bottom current velocities (equations (16) and (17)). The number of total prognostic equations is reduced to nine. Again, the equations are solved using Gear's method.

Figure 9a–d shows the transient solutions for the perturbation along-shelf winds, cross-shelf surface currents, mid-shelf upwelling and mid-shelf perturbation SST, respectively. During the first inertial day, the outer shelf along-shelf perturbation wind (v'_{a+}) for the rigid lid case (Fig. 9a) is almost identical to that of the free surface case (Fig. 7a). But the magnitude of v'_{a+} in the rigid lid case decreases more rapidly with time than in the free

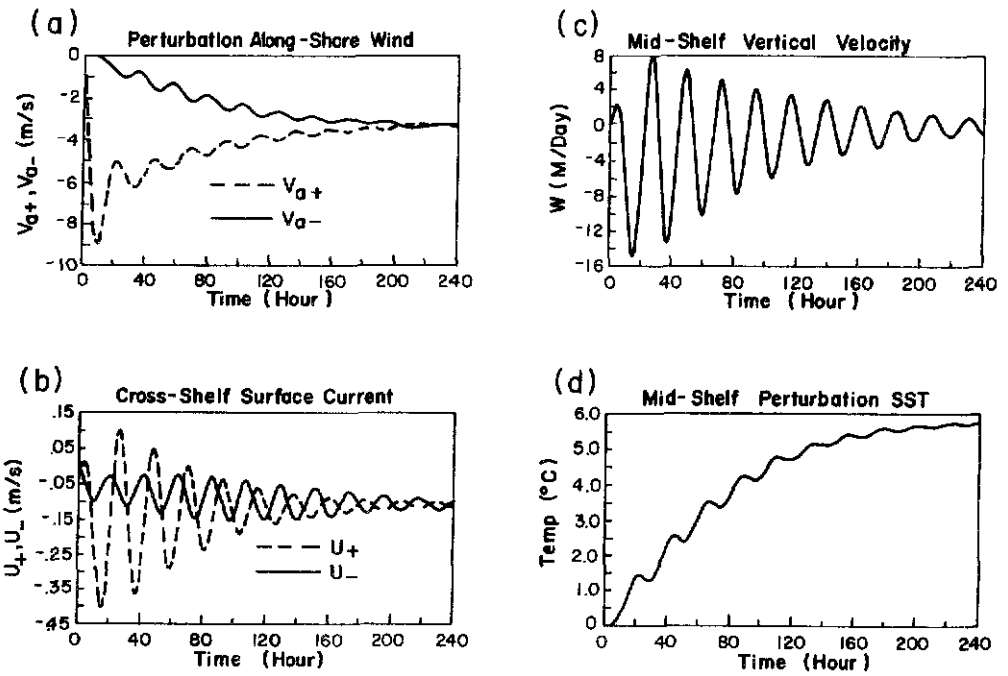

Fig. 9. Evolution of surface winds and ocean circulation in a coupled low-order model with constant Ekman layer depth ($k=0$) and rigid-lid approximation ($h_-=0$); (a) perturbation along-shelf surface wind speed over the inner shelf (solid curve) and the outer shelf (broken curve); (b) cross-shelf surface current speed over the inner shelf (solid curve) and the outer shelf (broken curve); (c) mid-shelf vertical velocity at the mid-depth; (d) mid-shelf perturbation SST.

surface case. As a result, at the end of the third inertial day, v'_{a+} is roughly 4.5 m s^{-1} which is approximately 0.5 m s^{-1} weaker than the corresponding value in the free surface case. The along-shelf perturbation wind over the inner shelf, on the other hand, increases more rapidly in the rigid lid case than in the free surface case. As a result, at the end of day three, it is roughly 0.5 m s^{-1} stronger in the rigid lid case than in the free surface case. Figure 9b shows the cross-shelf ocean currents in the rigid lid case. The onshore current over the outer shelf is roughly 5 cm s^{-1} stronger in the rigid lid case than in the free surface case during the first 2 days when the cross-shelf SST contrast between the mid- and outer-shelves are large. The cross-shelf currents over the inner shelf are similar in both cases which are stabilized at roughly 12 cm s^{-1} after day two. The other apparent difference between the two cases is that in the rigid lid case, the oscillation of the outer shelf current, has a larger amplitude initially, but is damped more rapidly than in the free surface case. Because of the large initial amplitude in the outer shelf current field, the mid-shelf downwelling rate also has a large amplitude initially in the rigid lid case (Fig. 9c). At steady state, we expect the mid-shelf downwelling rate to approach zero in all cases. Figure 9d shows the mid-shelf perturbation SST field. It evolves toward a steady state near $T'=5.2$°C, roughly 1 degree warmer than the free surface case.

Overall, in the rigid lid case, the inertial oscillation has a larger amplitude but is also

damped more rapidly than in the free surface case. At steady state, the mid-shelf SST is warmer in the rigid lid case than in the free surface case. An explanation for the weaker inner shelf current in the free surface case is that the sea level slope causes an offshore pressure gradient which partially balances the onshore forcing due to wind stress. This also results in a weaker cross-shelf current over the mid-shelf, which in the present model is the mean value between the inner and the outer shelves, and consequently is manifested by weaker onshore advection and a lower mid-shelf SST. Alternatively, we could conclude that the rigid lid approximation could over-predict the mid-shelf SST, inner shelf current and wind, while under predicting the outer shelf current and wind.

4.2. *The equilibrium wind approximation*

In this section, we will explore the transient behavior of the rigid lid model under some special circumstances. First, we assume the surface winds to always be in equilibrium with the cross-shelf SST gradient while other model variables are allowed to evolve according to their time-dependent governing equations. We will refer to such an assumption as the *equilibrium wind approximation*. This is equivalent to adopting the sea-breeze type circulation solution derived by Hsu (1984) for the atmosphere. Under this approximation, the number of prognostic equations reduces to 5 (See Appendix B).

Figure 10a shows the along-shelf winds over the inner and outer shelves. They are always in equilibrium with the respective cross-shelf SST gradient. The major difference between the equilibrium wind approximation (Fig. 10a) and the corresponding fully-

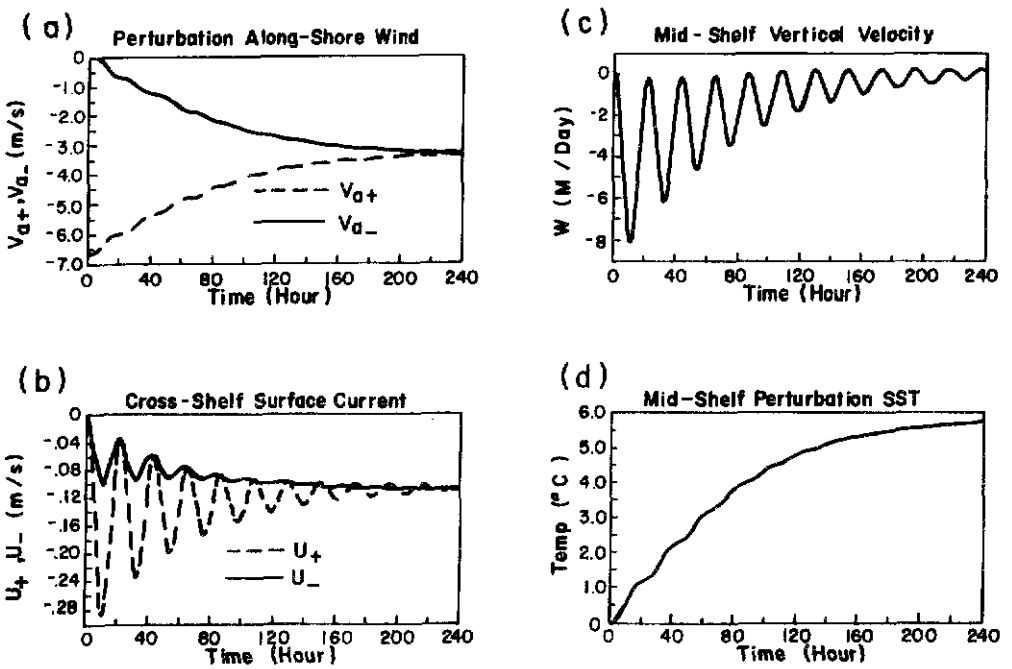

Fig. 10. Same as Fig. 9 but under equilibrium wind approximation.

coupled case (Fig. 9a) is that in the equilibrium wind case, the inertial oscillation is nearly filtered out and the initial along-shelf wind speed is $6.7\,m\,s^{-1}$. Qualitatively and quantitatively to first order, the results for the two cases are very similar except initially. Figure 10b shows the cross-shelf surface current over the inner and outer shelves. The current speed over the inner shelf is on the order of $0.11\,m\,s^{-1}$ which is similar to the corresponding fully-coupled case (Fig. 9b) except that the amplitude of the oscillation is damped more strongly in the equilibrium wind case, particularly over the inner shelf. The current speed over the outer shelf appears considerably weaker in the equilibrium wind case than in the corresponding fully-coupled case following the onset of the wind. For example, during the third inertial period, the peak outer-shelf current speed (which occurs at 60 h) is roughly $0.28\,m\,s^{-1}$ in the fully-coupled case while only $0.2\,m\,s^{-1}$ in the equilibrium wind case (occurring at 55 h). The mid-shelf upwelling rate is shown in Fig. 10c. Clearly, downwelling prevails during the early period but the maximum downwelling rate is weaker than that in the fully-coupled case (Fig. 9c). Figure 10d shows the mid-shelf perturbation SST. It increases in time with little oscillation. The lack of oscillation is obviously due to the filtering of inertial oscillations from the wind field by assuming it is in equilibrium with the SST field. At the end of day ten, when the equilibrium wind has already reached steady state, and the corresponding fully-coupled case has reached quasi-steady state, the difference between the two cases is very small. In fact, they should be identical at the true steady state. Thus, the major drawback with the equilibrium wind approximation is that it under-predicts the outer-shelf current speed, the mid-shelf downwelling rate, the SST, and consequently the outer-shelf along-shelf wind speed during the first 2–3 days.

4.3. *The equilibrium Ekman drift approximation*

The *equilibrium Ekman drift* approximation refers to the special case in which the surface ocean currents are always in equilibrium with the surface wind stress. The simplified model equations are given in Appendix C.

Figure 11a–d shows the perturbation surface along-shelf winds, surface cross-shelf currents, mid-shelf upwelling rate and perturbation SST, respectively. In this case, the along-shelf wind over the outer shelf (Fig. 11a) is very similar to the corresponding fully-coupled case (Fig. 9a), during the initial few days but displays little oscillation thereafter. The along-shelf wind over the inner shelf is completely void of oscillation and is generally weaker than that in the fully-coupled case, particularly during later times. At the end of day ten, the inner shelf wind is still much weaker than that over the outer shelf although they approach each other in the steady state. A similar situation happens for surface cross-shelf currents (Fig. 11c) since they are in equilibrium with the surface wind stress. Because of the lack of an oscillating component, the extreme currents are much weaker in Fig. 11c than in Fig. 9c, suggesting that the case of an equilibrium Ekman drift approximation also results in an under-prediction of cross-shelf currents during the early period, before oscillations are damped significantly. The mid-shelf perturbation SST is also under-predicted in the equilibrium Ekman drift approximation (Fig. 11d). At the end of day three, the difference of the mid-shelf SST between the equilibrium Ekman drift approximation and the fully-coupled case is roughly 1.5°C. Again, this difference decreases in time when the steady state value is approached.

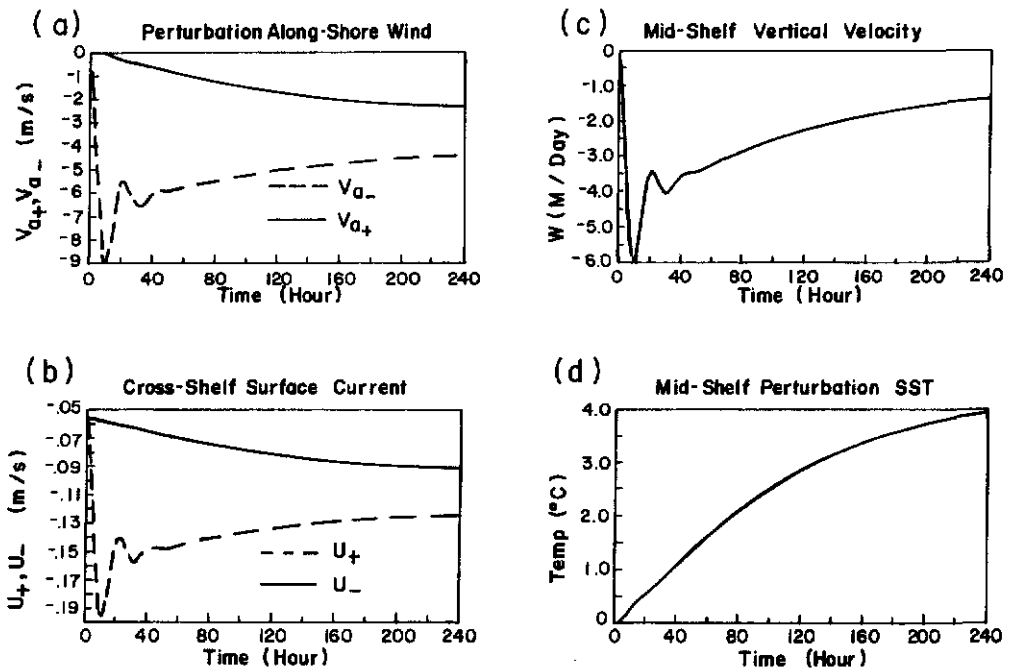

Fig. 11. Same as Fig. 9 but under equilibrium Ekman drift approximation.

4.4. *The fast coupling approximation: an analytical solution*

Assume that the surface ocean currents are *always* in equilibrium with the surface winds which, in turn, are always in equilibrium with SST gradient forcing. This assumption is equivalent to setting the left hand side of all equations, except that for the SST, to zero, which implies that the atmosphere and the ocean are "instantly" adjusted to each other. We will refer to this special situation as the *fast coupling* approximation. The only prognostic equation in this case is the thermodynamic equation which can be written as

$$dT'/dt + \beta T'^{2} + \gamma T' + c = 0 \tag{23}$$

where

$$T' = T - T_-,$$

$$\beta = -2AB/\delta x,$$

$$\gamma = AB(T_+ - T_-)/\delta x - \sigma,$$

$$c = 0.25B(T_+ - T_-)[(T_+ - T_-)A - 2v^*]\delta x - \sigma(T_- - T^*),$$

$$A = a(1 - \mu v/f^2),$$

$$v^* = (v_{am} + \nu u_{am}/f).$$

Equation (23) can be solved analytically. The solutions can be expressed as

$$T' = \begin{cases} \frac{\gamma-\sqrt{\Delta}-(\gamma+\sqrt{\Delta})\chi_1 e^{\sqrt{\Delta}t}}{2\beta(\chi_1 e^{\sqrt{\Delta}t}-1)}, & if\ \Delta > 0; \\ -\frac{2+\gamma(t-\chi_2)}{2\beta(t-\chi_2)}, & if\ \Delta = 0 \\ \frac{\sqrt{|\Delta|}\tan[\frac{\sqrt{|\Delta|}}{2}(t-\chi_3)]-\gamma}{2\beta}, & if\ \Delta < 0 \end{cases} \tag{24}$$

where

$$\chi_1 = \frac{2\beta T_0 + \gamma - \sqrt{\Delta}}{2\beta T_0 + \gamma + \sqrt{\Delta}},$$

$$\chi_2 = \frac{2}{2\beta T_0 + \gamma},$$

$$\chi_3 = \frac{2}{\sqrt{\Delta}} \arctan \frac{2\beta T_0 + \gamma}{\sqrt{\Delta}}$$

$$\Delta = \gamma^2 - 4\beta c,$$

and T_0 is the initial value of $T - T_-$. It can be easily shown that under northerly (southward) or weak southerly (northward) ambient wind, with other parameters given earlier, Δ is greater than zero. In this case, the steady state solution of T' is:

$$T'_e = -\frac{\gamma + \sqrt{\Delta}}{2\beta}$$

Since both A and B are positive, β must be negative. The value of γ is also positive since σ is usually less than $AB(T_+ - T_-)/\delta x$ which represents the inverse of the cross-shelf advective time scale. Thus, T'_e must be positive, i.e. an increase of mid-shelf SST. It can easily be shown that, at steady state, the mid-shelf SST increases with the coupling strength (AB). This is achieved through an increase of $-\Delta/4\beta^2$ which is equivalent to

$$3(T_+ - T_-)^2 + \sigma(AB\delta x)^{-2} - 2(T_+ - T_-)(\sigma/\delta x + 2v^* B)(AB)^{-1}.$$

The first term is the dominant term which represents the warming effect of the basic cross-shelf SST gradient on the mid-shelf SST. The second term is usually very small and can be neglected. The last term is negative and decreases in magnitude with the coupling strength (AB). It is also clear from the last term that a positive v^* (southerly ambient wind) reduces the mid-shelf warming effect, while a northerly ambient wind ($v^* < 0$) enhances mid-shelf warming. For larger σ (strong cooling), the steady state mid-shelf SST is lower, which is consistent with the physics.

Finally, we will compare the transient solution of the fast coupling case to that in the fully-coupled case. We find that, despite the lack of inertial oscillations, the solution is in better agreement with the fully coupled solution than are the equilibrium wind and equilibrium Ekman drift approximations. We will show the only prognostic variable, the mid-shelf perturbation SST (Fig. 12), to elaborate on this. At the end of the first three inertial days, the approximate mid-shelf SST values are respectively 1.5, 2.5 and 3.5°C in the fast coupling case. The corresponding values in the fully-coupled case are 1.4, 2.5, and 3.4°C (Fig. 9d). This suggests that "fast coupling" is a reasonably good

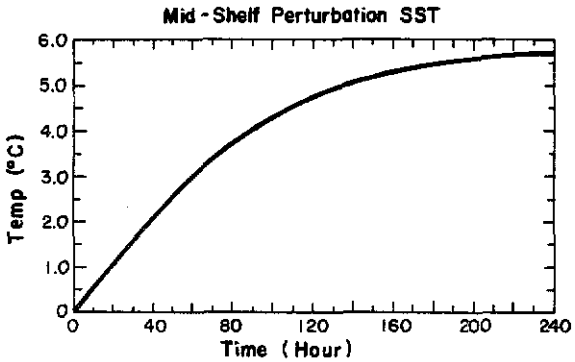

Fig. 12. Mid-shelf perturbation SST under the fast-coupling approximation.

approximation except that the inertial oscillation is completely filtered by the fast coupling approximation.

5. SENSITIVITY TO COUPLING STRENGTH AND AMBIENT WIND SPEED

In this section, we consider the sensitivity of the steady state solutions to the coupling strength and ambient wind speed. This will be exemplified by the variability of mid-shelf perturbation SST as a function of the coupling strength and ambient wind speed, respectively. Since the rigid lid approximation does not qualitatively alter the solution of the mid-shelf perturbation SST, we will, for simplicity, only discuss the rigid lid case. The steady state equation for mid-shelf perturbation SST ($T' = T - T_-$) can be derived as

$$\alpha T'^{3} + \beta_1 T'^{2} + \gamma_1 T' + c_1 = 0 \tag{25}$$

where

$$\alpha = -BAk/\delta x,$$
$$\beta_1 = 0.75\alpha(T_+ - T_-) - B(2A - kv^*)/\delta x,$$
$$\gamma_1 = -B(T_+ + T_-)1.25kv^* - A[1 + k(T_+ - T_-)]/\delta x - \sigma$$
$$c_1 = -0.25B(T_+ - T_-)2v^* + (T_+ - T_-)[k[v^* - A(T_+ - T_-)] - A]/\delta x - \sigma(T_- - T^*),$$
$$v^* = (v_{am} + \nu u_{am}/f).$$

If $k = 0$, i.e. assuming a constant Ekman layer depth, then $\alpha = 0$, $\beta_1 = \beta$, $\gamma_1 = \gamma$, and $c_1 = c$.

5.1. *Sensitivity to coupling strength*

In equation (25), the strength of air–sea coupling is described by the values of A and B which are determined by the thermal response coefficient Π, drag coefficient r, and the friction coefficients μ and ν. For fixed drag coefficient and friction coefficients, the coupling strength is determined by Π or equivalently A. Thus, we will use A as an external parameter to examine the sensitivity of the steady state mid-shelf perturbation SST to air–sea coupling strength. Other model parameters are the same as those used earlier.

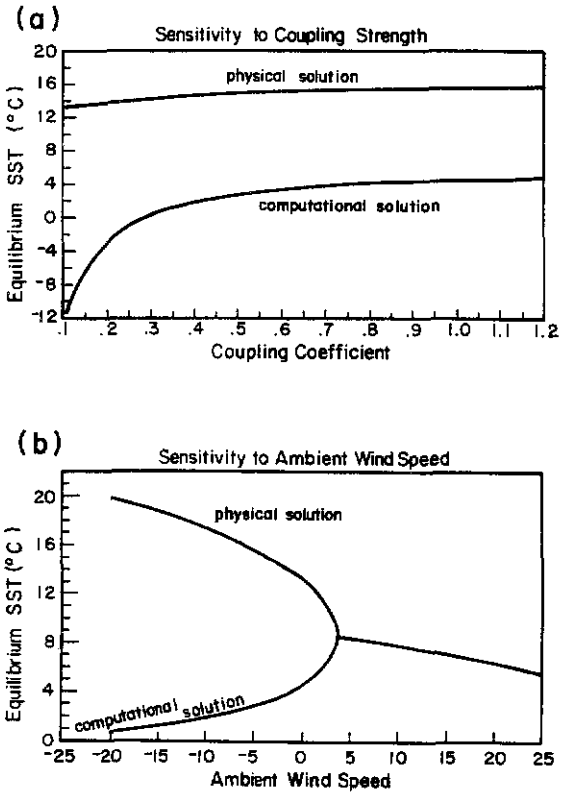

Fig. 13. Sensitivity to model parameters. (a) Sensitivity of mid-shelf SST to coupling strength; (b) Sensitivity of mid-shelf SST to ambient wind speed.

Figure 13a shows the steady state solution for the mid-shelf SST as a function of A. In general, the value of A is positive. This is easily seen from the definition of A (Section 4, and Appendix B), since a higher SST induces lower surface atmospheric pressure so the atmospheric pressure gradient induced by an oceanic front must be in the opposite direction to the SST gradient, and thus the surface perturbation winds must blow from cold water toward warm water. Figure 13a shows that T varies from roughly 13°C for $A = 0.1\ \mathrm{m\ s^{-1}\ deg^{-1}}$ to 15°C for $A = 1.2\ \mathrm{m\ s^{-1}\ deg^{-1}}$. The variance of the steady state T is roughly 2°C over an order of magnitude range of A. We conclude that mid-shelf perturbation SST can be affected by the coupling strength (here determined by A). The stronger the coupling the larger is the mid-shelf perturbation SST. Alternatively, we may qualitatively state that the steady state value of T is significantly affected by air–sea coupling.

5.2. *Sensitivity to ambient wind speed*

Now consider the effect of ambient wind speed on the steady state solutions. The coupling strength in this case is the same as that used in Section 3 and Section 4. The steady state mid-shelf SST is shown in Fig. 13b as a function of v_{am}. It is interesting to note that a physical

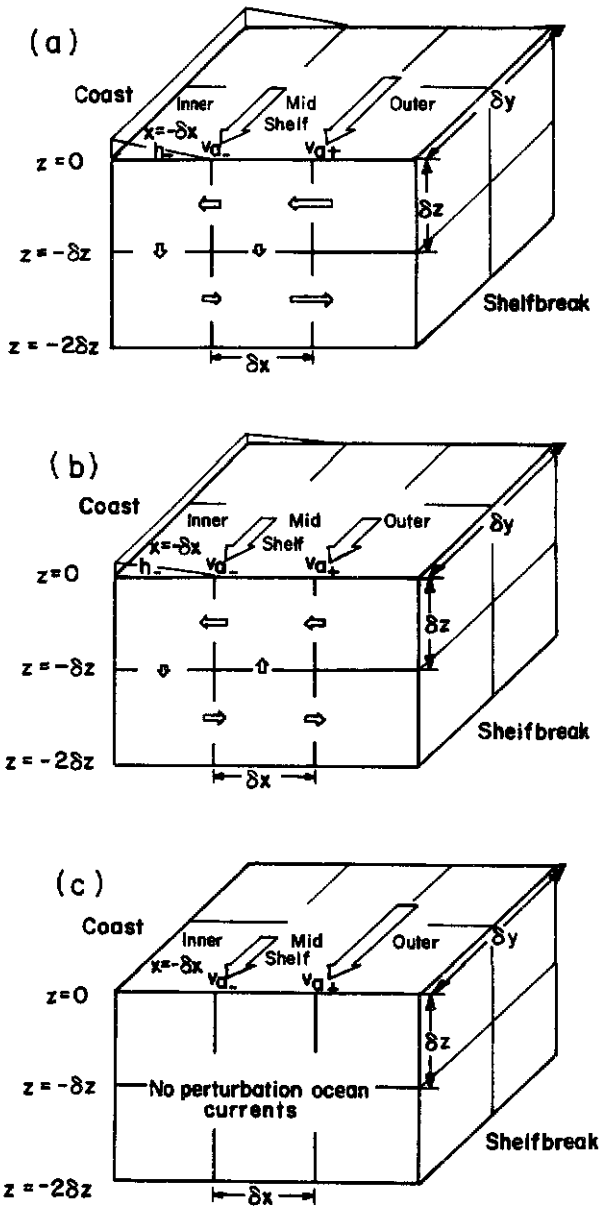

Fig. 14. Schematic representation of the surface wind and ocean circulation in coupled and uncoupled models; (a) coupled; (b) constant wind; (c) constant SST and ocean circulation.

solution exists only when v_{am} is less than a critical value (v_{ac}) of roughly 4 m s^{-1}, when v_{am} becomes northward. The SST in the mid-shelf is proportional to the speed of the southward component of the ambient wind. The value of T varies from 8.5°C for a weak northward ambient wind of roughly 4 m s^{-1} to about 20°C for a 25 m s^{-1} southward ambient wind. It

is clear that the SST in the mid-shelf is sensitive to the ambient wind speed. Such a sensitivity decreases, however, as the speed of the southward ambient wind increases and the mid-shelf SST approaches T_+.

6. DISCUSSION AND CONCLUSIONS

Although no observations were available for quantitative verification of the coastal sea-level change, bottom current velocity and upwelling rates generated by the model, qualitatively, the cross-shelf circulation pattern and coastal sea-level change in the model (schematically depicted in Fig. 14a) are consistent with the "Ekman frictional equilibrium response" to local along-shelf wind forcing (Beardsley and Butman, 1974; Scott and Csanady, 1976) which is often observed on continental shelves (Beardsley and Winant, 1979; Hickey and Hamilton, 1980; Mitchum and Sturges, 1982; Lee *et al.*, 1984, 1989). The surface wind pattern resembles the sea-breeze type circulations in 2-D (Hsu, 1984).

The rigid lid approximation generally over-estimates the intensity of shelf circulation, surface wind speed and mid-shelf SST. Among the three types of equilibrium assumptions, i.e. the equilibrium wind, equilibrium Ekman drift, and fast coupling approximations, the equilibrium Ekman drift approximation seems to be the least promising choice, while the equilibrium wind approximation is closest to the fully-coupled model. It is also shown that the fast coupling approximation is not an unreasonable choice although it filters out the inertial oscillation completely.

We have studied the sea surface temperature, ocean currents and surface winds in a coupled low-order model with various approximations. The model has only minimal resolution in the cross-shelf direction and is essentially uniform in the along-shelf direction. The main feedback processes between the atmosphere and the ocean are via the surface and bottom Ekman drift layers induced by winds and friction and the atmospheric pressure gradient induced by the cross-shelf SST gradient. Results from the control experiment and the uncoupled experiment indicate that air–sea coupling is important for sub-synoptic scale wind, SST and ocean current variability over continental shelves similar to the South Atlantic Bight environment. It is important to point out that if surface winds are not affected by SST, then surface winds and currents over the shelf would be weaker than their counterparts in the coupled system during northerly ambient wind conditions (Fig. 14b), suggesting that the effect of SST on the atmosphere enhances coastal ocean circulation. However, if on the other hand, we assume the SST is not affected by the surface wind field, then a warm SST anomaly (e.g. a Gulf Stream frontal feature) near the shelf break during typical wintertime southward wind conditions would maintain a large cross-shelf SST gradient between the mid- and outer shelves since no warm water is advected onto the mid-shelf by winds. This large cross-shelf SST gradient can induce a stronger southward surface wind on the outer shelf (just shoreward of the shelfbreak SST front) than its counterpart in the coupled system. In other words, air–sea coupling reduces the strength of the ocean circulation and the along-shelf surface wind speed over the outer shelf (Fig. 14c). In the coupled system, cross-shelf SST gradient enhances the along-shelf wind which in turn warms the mid-shelf. The warming of the mid-shelf enhances the cross-shelf SST gradient over the inner shelf but reduces the cross-shelf SST gradient over the outer shelf. This causes an asymmetry in the along-shelf surface wind field. Under northerly ambient wind conditions, its intensity over the outer-shelf becomes weaker than that in models with prescribed SST but stronger than the ambient wind speed, while over the inner shelf, the

along-shelf wind is stronger than the ambient wind speed as well as the along-shelf wind speed in models with prescribed SST.

In this low-order model, air–sea interaction does not result in instability. The coupled circulation reaches equilibrium state eventually. This is because in the present model the cross-shelf SST gradient induces a cross-shelf pressure gradient in the atmosphere which creates an opposite tendency in the wind fields on each side of the maximum SST gradient. Thus the part of the along-shelf wind associated with an increase of mid-shelf SST is accelerated (or decelerated) in opposite directions over the inner shelf (southward acceleration) and the outer shelf (southward deceleration or northward acceleration) which eventually discourages further mid-shelf warming (Fig. 2).

7. FINAL REMARKS

A theory has been proposed which suggests that air–sea interaction is important for low-level coastal winds and the associated continental shelf ocean circulation. Both cross-shelf and along-shelf variability of the coastal atmosphere and coastal ocean should be considered in order to understand the coupled behavior of the coastal sea–air system more fully. Further investigation of the coupled response using atmospheric and ocean models with more realistic physics has been conducted and the results will be presented in subsequent papers.

The low-order model used in this study is simple, and is not intended to represent the real coastal sea–air system accurately and quantitatively. Thus, caution must be taken when applying the results to real coastal systems. However, as Vallis (1990) pointed out, "By applying maximum simplification, some criticism has been laid at the foot of such low order models for being overly simplistic. Such criticism is fair if the models are demonstrably unphysical. However, low order models can be useful in laying bare the essential physics, or shaving away the unessential." We believe that Vallis' point is well taken.

Acknowledgements—This study was supported by the Department of Energy's Atmospheric Radiation Measurements program under Grant #091575-A-Q1 with Pacific Northwest Laboratories Atmospheric Sciences Division (to S. Raman) and to the Department of Energy's Ocean Margin Program under Grant #DEFG0985ER60376 (to L.J. Pietrafesa). L. Salzillo drafted the figures and B. Batts conducted the word processing.

REFERENCES

Atkinson, L. P., Lee, T. N., Blanton, J. O. and Chandler, W. S. (1983) Climatology of the southeastern United States continental shelf waters. *Journal of Geophysical Research (Oceans)* **88**, 4705–4718.

Atkinson, L. P., Oka, E., Wu, S. Y., Berger, T. J., Blanton, J. O. and Lee, T. N. (1989) Hydrographic variability of Southeastern United States shelf and slope waters during the Genesis of Atlantic Lows Experiment: winter 1986. *Journal of Geophysical Research (Oceans)* **94**, 10699–10713.

Beardsley, R. C. and Butman, B. (1974) Circulation on the New England continental shelf: response to strong winter storms. *Geophysical Research Letters* **1**, 181–184.

Beardsley, R. C. and Winant, C. D. (1979) On the mean circulation in the Mid-Atlantic Bight. *Journal of Physical Oceanography* **9**, 612–619.

Bumpus, F. (1973) The circulation of the circulation on the continental shelf of the east coast of the U.S *Progress in Oceanography* **6**, 111–157.

Cane, M. A. and Zebiak, S. E. (1985) A theory for El Nino and the Southern Oscillation. *Science* **28**, 1084–1087.

Charney, J. G. and DeVore, J. G. (1979) Multiple flow equilibria in the atmosphere and blocking. *Journal of Atmospheric Science* **36**, 1205–1216.

Doyle, J. D. and Warner, T. T. (1990) Mesoscale coastal processes during GALE IOP 2. *Monthly Weather Review* **118**, 283–308.

Doyle, J. D. and Warner, T. T. (1993) A three-dimensional numerical investigation of a Carolina coastal low-level jet during GALE IOP 2. *Monthly Weather Review* **121**, 1030–1047.

Gear, C. W. (1971) *Numerical Initial-value Problems in Ordinary Differential Equations*. Prentice-Hall, Englewood Cliffs, NJ.

Hickey, B. M. and Hamilton, P. (1980) A spin-up model as a diagnostic tool for interpretation of current and density measurements on the continental shelf of the Pacific northwest. *Journal of Physical Oceanography* **10**, 12–24.

Hsu, S. A. (1984) Sea-breeze-like winds across the north wall of the Gulf Stream: An analytical model. *Journal of Geophysical Research* **89**, 2025–2028.

Hsu, S. A. (1988) *Coastal Meteorology*. Academic Press, New York.

Huang, C.-Y. and Raman, S. (1992) A three-dimensional numerical investigation of a Carolina coastal front and Gulf Stream rainband. *Journal of Atmospheric Science* **49**, 560–584.

Janowitz, G. S. and Pietrafesa, L. J. (1980) A model and observations of time dependent upwelling over the mid-shelf and slope. *Journal of Physical Oceanography* **10**(10), 1574–1583.

Klinck, J. M., Pietrafesa, L. J. and Janowitz, G. S. (1981) On the continental shelf circulation induced by a moving, localized wind stress. *Journal of Physical Oceanography* **11**, 836–848.

Lau, K.-M. (1981) Oscillations in a simple equatorial climate system. *Journal of Atmospheric Science* **38**, 248–261.

Lee, T. N., Ho, W. J., Kourafalou, V. and Wang, J. D. (1984) Circulation on the Southeast U.S. continental shelf, I., Subtidal response to wind and Gulf Stream forcing. *Journal of Physical Oceanography* **14**, 1001–1012.

Lee, T. N., Kourafalou, V., Wang, J. D., Ho, W. J., Blanton, J. O., Atkinson, L. P. and Pietrafesa, L. J. (1985) Shelf circulation from Cape Canaveral to Cape Fear during winter. Oceanography of the Southeastern U.S. Continental Shelf. Coastal and Estuarine Sciences **2**, 33–62. *American Geophysical Union.*

Lee, T. N., Williams, E., Wang, J., Evans, R. and Atkinson, L. (1989) Response of South Carolina continental shelf waters to wind and Gulf Stream forcing during winter of 1986. *Journal of Geophysical Research (Oceans)* **94**, 10715–10754.

Lorenz, E. N. (1963) Deterministic nonperiodic flow. *Journal of Atmospheric Science* **20**, 130–141.

Mahrt, L. and Paumier, J. (1982) Cloud-top entrainment instability observed in AMTEX. *Journal of Atmospheric Science* **33**, 41–45.

McWilliams, J. C. and Gent, P. R. (1978) A coupled air and sea model for the tropical Pacific. *Journal of Atmospheric Science* **35**, 962–989.

Mitchum, G. T. and Sturges, W. (1982) Wind-driven currents on the west Florida shelf. *Journal of Physical Oceanography* **12**, 1310–1317.

Pietrafesa, L. J. (1989) The Gulf Stream and wind events on the Carolina Capes shelf. NOAA-NURP (National Undersea Research Program) Research Report **89-2**, pp. 89–129.

Pietrafesa, L. J. and Janowitz, G. S. (1980) On the dynamics of the Gulf Stream front in the Carolina Capes. In *Proceedings of the 2nd International Symposium on Stratified Flows*, pp. 184–187. Trondheim, Norway, 24–27 June, 1980, Tapin Publishing Co.

Pietrafesa, L. J., Janowitz, G. S. and Wittman, P. A. (1985) Physical oceanographic processes in the Carolina Capes. Oceanography of the Southeastern U.S. Continental Shelf. Coastal and Estuarine Sciences **2**, pp. 23–32. *American Geophysical Union.*

Riordan, A. J. and Lin, Y.-L. (1992) Mesoscale wind signatures along the Carolina Coast. *Monthly Weather Review* **120**, 2786–2797.

Suarez, M. J. and Schopf, P. S. (1988) A delayed action oscillator for ENSO. *Journal of Atmospheric Science* **45**, 3283–3287.

Scott, J. T. and Csanady, G. T. (1976) Nearshore currents off Long Island. *Journal of Geophysical Research (Oceans)* **81**, 5401–5409.

Sweet, W., Fett, R., Kerling, J. and La Violette, P. (1981) Air–sea interaction effects in the lower troposphere across the north wall of the Gulf Stream. *Monthly Weather Review* **109**, 1042–1052.

Vallis, G. K. (1986) El Nino, A chaotic dynamical system? *Science* **232**, 243–245.

Vallis, G. K. (1990) Conceptual models of El Nino and Southern Oscillation. *Journal of Geophysical Research* **95**, 13797–13809.

Weisberg, R. H. and Pietrafesa, L. J. (1983) Kinematics and correlation of the surface wind field of the South Atlantic Bight. *Journal of Geophysical Research* **88**(C8), 4593–4610.

Xie, L. and Pietrafesa, L. J. (1995) Shoreward intrusion of upper Gulf Stream warm water by prescribed shelfbreak temperature perturbation and surface wind stress. *Geophysical Research Letters* **22**, 2585–2588.

APPENDIX A

Model equations of the rigid lid case

In this case, we can derive a set of equations for the symmetric and antisymmetric portions of the surface perturbation wind and current fields.

Consider first the transient solutions under the assumptions of rigid lid, $k=0$, and $V_-^N = V_-$. Let

$$\begin{aligned} X_1 &= T + T_- \\ X_2 &= U_+ + U_- \\ X_3 &= U_+ - U_- \\ X_4 &= V_+ + V_- \\ X_5 &= V_+ - V_- \\ X_6 &= u_{a+} + u_{a-} \\ X_7 &= u_{a+} - u_{a-} \\ X_8 &= v_{a+} + v_{a-} \\ X_9 &= v_{a+} - v_{a-} \end{aligned} \tag{A1}$$

Then the model equations can be rewritten as

$$\begin{aligned} dX_1/dt &= a_{11}X_3 + a_{12}X_2 + b_{13}X_3 + c_1 \\ dX_2/dt &= a_{22}X_2 + a_{24}X_4 + a_{26}X_6 + c_2 \\ dX_3/dt &= a_{33}X_3 + a_{35}X_5 + a_{37}X_7 \\ dX_4/dt &= a_{42}X_2 + a_{44}X_4 + a_{48}X_8 + c_4 \\ dX_5/dt &= a_{53}X_1 + a_{55}X_3 + a_{59}X_9 \\ dX_6/dt &= a_{66}X_6 + a_{68}X_8 + c_6 \\ dX_7/dt &= a_{71}X_1 + a_{77}X_7 + a_{79}X_9 + c_7 \\ dX_8/dt &= a_{86}X_6 + a_{88}X_8 \\ dX_9/dt &= a_{97}x_7 + a_{99}X_9 \end{aligned} \tag{A2}$$

where

$$\begin{aligned} a_{11} &= -\sigma \\ a_{12} &= -0.25(T_+ - T_-)/\delta x \\ a_{22} &= a_{33} = a_{44} = a_{55} = -\nu \\ a_{24} &= a_{35} = a_{68} = a_{79} = f \\ a_{26} &= a_{37} = a_{48} = a_{59} = r/D \\ a_{42} &= a_{53} = a_{86} = a_{97} = -f \\ a_{66} &= a_{77} = a_{88} = a_{99} = -\mu \\ a_{71} &= -2\pi \\ b_{13} &= -1/\delta x \\ c_1 &= \sigma(T^* - T_-) \\ c_2 &= 2ru_{am}/D \\ c_4 &= 2rv_{am}/D \\ c_6 &= \Pi(T_+ - T_-) \\ c_7 &= \Pi(T_+ + 3T_-) \end{aligned}$$

Again the Gear's method is used here to solve equation (A2).

APPENDIX B

Model equations for the equilibrium wind case

Let

$$\begin{aligned} X_1 &= T + T_- \\ X_2 &= U_+ + U_- \\ X_3 &= U_+ - U_- \\ X_4 &= V_+ + V_- \\ X_5 &= V_+ - V_- \end{aligned} \tag{B1}$$

The model equations can be rewritten as

$$\begin{aligned} dX_1/dt &= a_{11}X_3 + a_{12}X_2 + b_{13}X_1X_3 + c_1 \\ dX_2/dt &= a_{22}X_2 + a_{24}X_4 + c_2 \\ dX_3/dt &= a_{31}X_1 + a_{33}X_3 + a_{35}X_5 + c_3 \\ dX_4/dt &= a_{42}X_2 + a_{44}X_4 + c_4 \\ dX_5/dt &= a_{51}X_1 + a_{53}X_3 + a_{55}X_3 + c_5 \end{aligned} \tag{B2}$$

where

$$\begin{aligned} a_{11} &= -\sigma \\ a_{12} &= -0.25(T_+ - T_-)/\delta x \\ a_{22} &= a_{33} = a_{44} = a_{55} = -\nu \\ a_{24} &= a_{35} = f \\ a_{31} &= -2ar\mu/fD \\ a_{42} &= a_{53} = -f \\ a_{51} &= 2ar/D \\ b_{13} &= -1/\delta x \\ c_1 &= \sigma(T^* - T_-) \\ c_2 &= r[2u_{am} + \mu a(T_+ - T_-)/f]/D \\ c_3 &= ar\mu(T_+ - T_-)/D/f \\ c_4 &= r[2v_{am} - a(T_+ - T_-)]/D \\ a &= \Pi[f(1 + \mu^2/f^2]^{-1} \end{aligned}$$

APPENDIX C

Model equations for the Ekman equilibrium approximation

Similar to the derivation of equation (B2), we can easily find the governing equations by defining

$$\begin{aligned} X_1 &= T + T_- \\ X_2 &= u_{a+} + u_{a-} \\ X_3 &= u_{a+} - u_{a-} \\ X_4 &= v_{a+} + v_{a-} \\ X_5 &= v_{a+} - v_{a-} \end{aligned} \tag{C1}$$

The model equations can be rewritten as

$$\begin{aligned} dX_1/dt &= a_{11}X_3 + a_{12}X_2 + a_{14}X_4 + b_{13}X_1X_3 + b_{15}X_1X_5 + c_1 \\ dX_2/dt &= a_{22}X_2 + a_{24}X_4 + c_2 \\ dX_3/dt &= a_{31}X_1 + a_{33}X_3 + a_{35}X_5 + c_3 \\ dX_4/dt &= a_{42}X_2 + a_{44}X_4 \\ dX_5/dt &= a_{53}X_1 + a_{55}X_3 \end{aligned} \tag{C2}$$

where

$$\begin{aligned} a_{11} &= -\sigma \\ a_{12} &= -0.25\nu B(T_+ - T_-)/\delta x \\ a_{14} &= -0.25B(T_+ - T_-)/\delta x \\ a_{22} &= a_{33} = a_{44} = a_{55} = -\mu \\ a_{24} &= a_{35} = f \\ a_{31} &= -2\Pi \\ a_{42} &= a_{53} = -f \\ b_{13} &= -B\nu/f\ \delta x \\ b_{15} &= -\beta/\delta x \\ c_1 &= \sigma(T^* - T_-) - 0.5B(v_{am} + u_{am}\nu/f)/\delta x \\ c_2 &= \Pi(T_+ - T_-) \\ c_3 &= \Pi(T_+ + 3T_-) \\ B &= r/[fD(1 + \nu^2/f^2)] \end{aligned}$$

Unlinked references Xie and Pietrafesa, 1985 in references but year is 1995 in citation. Please advise correct year.The following were in the references but not cited in the manuscript. Please advise locations for citations:Hauwritz, 1947no linkPietrafesa, 1983no linkWinant *et al.*, 1987no link